Dalton Transactions

Accepted Manuscript

ROYAL SOCIETY OF CHEMISTRY

www.rsc.org/dalton

Submitted to Dalton Trans. as an article, January 14, 2015

<<Revised version on DT-ART-01-2015-000166>>

The effect of chlorine and fluorine substitutions on tuning the ionization potential of benzoate-bridged paddlewheel diruthenium(II, II) complexes†

Wataru Kosaka,[a,b] Masahisa Itoh[b] and Hitoshi Miyasaka,*[a,b]

[a] Institute for Materials Research, Tohoku University, 2-1-1 Katahira, Aoba-ku, Sendai 980-8577, Japan. E-mail: miyasaka@imr.tohoku.ac.jp

[b] Department of Chemistry, Graduate School of Science, Tohoku University, 6-3 Aramaki-Aza-Aoba, Aoba-ku, Sendai 980-8578, Japan

† Electronic supplementary information (ESI) available: Syntheses of several benzoate ligands, crystallographic data, ORTEP drawings of several compounds, magnetic data, a total plot of $E_{1/2}$ vs. $\Sigma(x\sigma_m + y\sigma_p + z\sigma_o)$ for the Cl-, F- and Me-series reported, plots of HOMO level vs. $E_{1/2}$ for the Cl-series and the F-series representing the average dihedral angle. CCDC reference numbers 1041309–1041325. For ESI and crystallographic data in CIF or other electronic formats, see DOI: XXXXXXXX.

Abstract

A series of paddlewheel diruthenium(II, II) complexes with various chlorine-substituted benzoate ligands (Cl-series) was synthesized as tetrahydrofuran (THF) adducts $[Ru_2(Cl_xPhCO_2)_4(THF)_2]$; where $Cl_xPhCO_2^-$ = *o*-chlorobenzoate, ***o*-Cl**; *m*-chlorobenzoate, ***m*-Cl**; *p*-chlorobenzoate, ***p*-Cl**; 2,3-dichlorobenzoate, **2,3-Cl_2**; 2,4-dichlorobenzoate, **2,4-Cl_2**; 2,5-dichlorobenzoate, **2,5-Cl_2**; 2,6-dichlorobenzoate, **2,6-Cl_2**; 3,4-dichlorobenzoate, **3,4-Cl_2**; 3,5-dichlorobenzoate, **3,5-Cl_2**; 2,3,4-trichlorobenzoate, **2,3,4-Cl_3**; 2,3,5-trichlorobenzoate, **2,3,5-Cl_3**; 2,4,5-trichlorobenzoate, **2,4,5-Cl_3**; 3,4,5-trichlorobenzoate, **3,4,5-Cl_3**; 2,3,4,5-tetrachlorobenzoate, **2,3,4,5-Cl_4**. This Cl-series and the previously synthesized F-series together with four new fluorine-substituted derivatives, $[Ru_2(F_xPhCO_2)_4(THF)_2]$ (where $F_xPhCO_2^-$ = 2,3-difluorobenzoate, **2,3-F_2**; 2,4-difluorobenzoate, **2,4-F_2**; 2,5-difluorobenzoate, **2,5-F_2**; 2,3,5-trifluorobenzoate, **2,3,5-F_3**), were experimentally characterized with respect to solid-state structure, magnetic properties and electrochemistry. By tuning the substituents of the benzoate ligands using chlorine or fluorine atoms, the redox potential ($E_{1/2}$) for $[Ru_2^{II,II}]/[Ru_2^{II,III}]^+$ varied over a wide range of potentials from −40 mV to 360 mV (vs. Ag/Ag^+ in THF). This was dependent on (i) the number of *ortho*-substituents, i.e. non-, mono- and di-*o*-substituted groups, with quasi-Hammett parameters for *ortho*-Cl and -F substitutions (σ_o = −0.272 and–0.217, respectively) and (ii) the general Hammett constants, σ_m and σ_p, for each group. The HOMO energy level calculated on the basis of the atomic coordinates of the solid-state structure was strongly affected by Cl- and F-substitutions as well as the redox potential in solution, which emphasizes the steric contribution of *ortho*-substituents in the energy level giving a deviation of $E_{HOMO} < 0.3$ eV and < 0.55 eV for the Cl- and F-series, respectively.

Introduction

Charge-transfer complexes composed of electron donor (D) and acceptor (A) units have attracted much attention as functional molecular materials that exhibit magnetic long-range ordering,[1] high conductivity,[2] ferroelectric properties[3] and synergistic functionalities.[4] When choosing D/A sets, the most important issue to consider is the control of the charge-transfer (D□A) followed by the occurrence of electron transfer from the neutral state (D^0A^0) to the ionic state ($D^{\delta+}A^{\delta-}$), which is largely affected by the ionization potential (I_D) of D and the electron affinity (E_A) of A.

Our groups have chosen a family of carboxylate-bridged paddlewheel diruthenium(II, II) complexes, $[Ru_2^{II,II}(RCO_2)_4]$ (abbreviated as $[Ru_2^{II,II}]$), as D for constructing covalently assembled D_mA_n frameworks with 7,7,8,8-tetracyano-*p*-quinodimethane (TCNQ) and *N*,*N'*-dicyanoquinodiimine (DCNQI) derivatives.[5] We have chosen these complexes on the basis of the following: i) $[Ru_2^{II,II}]$ itself also acts as a coordinating acceptor, while TCNQ and DCNQI derivatives act as coordinating donors, which are needed to construct the framework; ii) $[Ru_2^{II,II}]$ and its oxidation species $[Ru_2^{II,III}]^+$ are paramagnetic, with $S = 1$ and $S = 3/2$, respectively, i.e. both species are useful as magnetic building blocks; iii) the I_D of these complexes is accurately tuneable by modifying the carboxylate-bridging groups; and iv) the HOMO of the $[Ru_2^{II,II}]$ family is located at an energy level close to the LUMO of TCNQ and DCNQI, with an adequate energy gap between the HOMO of D and the LUMO of A.[6] Focusing on these benefits, DA- and D_2A-type compounds of $[Ru_2]$/TCNQ, DCNQI in multi-dimensional frameworks have been synthesized by tuning the intra-framework charge transfer/electron transfer in order to design magnetic and conducting materials.[5,6]

The ionization potential is a key factor for the rational design of charge transfer/electron transfer frameworks, as well as tuning of the E_A of the acceptor units (i.e. TCNQ and DCNQI derivatives)

used. In our previous work, we demonstrated that the donor character (i.e. I_D) of fluorine-substituted benzoate-bridged [$Ru_2^{II,II}$] complexes, [$Ru_2^{II,II}(F_xPhCO_2)_4(THF)_2$], is systematically affected depending on the position and number of substituted fluorine groups. This was analysed by electrochemistry, HOMO levels calculated on the basis of the atomic coordinates of the crystal structure and the Hammett law.[7] Here, we present a series of [$Ru_2^{II,II}$] complexes with various chlorine-substituted benzoate ligands, [$Ru_2(Cl_xPhCO_2)_4(THF)_2$], where $Cl_xPhCO_2^-$ = *o*-chlorobenzoate, ***o*-Cl**; *m*-chlorobenzoate, ***m*-Cl**; *p*-chlorobenzoate, ***p*-Cl**; 2,3-dichlorobenzoate, **2,3-Cl_2**; 2,4-dichlorobenzoate, **2,4-Cl_2**; 2,5-dichlorobenzoate, **2,5-Cl_2**; 2,6-dichlorobenzoate, **2,6-Cl_2**; 3,4-dichlorobenzoate, **3,4-Cl_2**; 3,5-dichlorobenzoate, **3,5-Cl_2**; 2,3,4-trichlorobenzoate, **2,3,4-Cl_3**; 2,3,5-trichlorobenzoate, **2,3,5-Cl_3**; 2,4,5-trichlorobenzoate, **2,4,5-Cl_3**; 3,4,5-trichlorobenzoate, **3,4,5-Cl_3**; 2,3,4,5-tetrachlorobenzoate, **2,3,4,5-Cl_4**; THF = tetrahydrofuran (Chart 1). The chlorine atom is known as a substituent with an electron-withdrawing effect which is similar to the fluorine atom but has slightly different properties owing to its higher electron affinity and larger atomic radius. We also added new fluorine-substituted derivatives, [$Ru_2(F_xPhCO_2)_4(THF)_2$], in order to increase the number of compounds in the series for comparison with the Cl-series, where $F_xPhCO_2^-$ = 2,3-difluorobenzoate, **2,3-F_2**; 2,4-difluorobenzoate, **2,4-F_2**; 2,5-difluorobenzoate, **2,5-F_2**; 2,3,5-trifluorobenzoate, **2,3,5-F_3** (Chart 1). All compounds were characterized by single-crystal X-ray analyses, magnetic properties and electrochemical properties measured in THF. Finally, the relationship between the electron-donating ability of [$Ru_2^{II,II}$] units and their chemical properties, such as pK_a, redox potential and the HOMO energy level calculated by density functional theory (DFT), was investigated in comparison with the F-series (Chart 1).

<<Insert Chart 1 here>>

Experimental Section

General Procedures and Materials

All synthetic procedures were performed under an inert atmosphere using standard Schlenk line techniques and a commercial glovebox.[7] All chemicals were reagent grade purchased from commercial sources. Solvents were dried using common drying agents and distilled under nitrogen before use. $[Ru_2^{II,III}(CH_3CO_2)_4(THF)_2]BF_4$,[8] $[Ru_2^{II,III}(CH_3CO_2)_4Cl]$[9] and several benzoic acids (*R*-PhCOOH, *R* = **2,3,4-Cl$_3$**, **2,3,5-Cl$_3$**, **2,4,5-Cl$_3$** and **3,4,5-Cl$_3$**)[10] were prepared by methods noted in the electronic supporting information and modified from a general procedure previously reported.[7]

Synthesis of $[Ru_2^{II,II}(o\text{-}ClPhCO_2)_4(THF)_2]$ (*o*-Cl), $[Ru_2^{II,II}(m\text{-}ClPhCO_2)_4(THF)_2]$ (*m*-Cl), $[Ru_2^{II,II}(2,3\text{-}Cl_2PhCO_2)_4(THF)_2]$ (2,3-Cl$_2$), $[Ru_2^{II,II}(2,4\text{-}Cl_2PhCO_2)_4(THF)_2]$ (2,4-Cl$_2$), $[Ru_2^{II,II}(2,5\text{-}Cl_2PhCO_2)_4(THF)_2]$ (2,5-Cl$_2$), $[Ru_2^{II,II}(2,6\text{-}Cl_2PhCO_2)_4(THF)_2]$ (2,6-Cl$_2$), $[Ru_2^{II,II}(3,4\text{-}Cl_2PhCO_2)_4(THF)_2]$ (3,4-Cl$_2$), $[Ru_2^{II,II}(3,5\text{-}Cl_2PhCO_2)_4(THF)_2]$ (3,5-Cl$_2$), $[Ru_2^{II,II}(2,3,4\text{-}Cl_3PhCO_2)_4(THF)_2]$ (2,3,4-Cl$_3$), $[Ru_2^{II,II}(2,3,5\text{-}Cl_3PhCO_2)_4(THF)_2]$ (2,3,5-Cl$_3$), $[Ru_2^{II,II}(2,4,5\text{-}Cl_3PhCO_2)_4(THF)_2]$ (2,4,5-Cl$_3$), $[Ru_2^{II,II}(2,5\text{-}F_2PhCO_2)_4(THF)_2]$ (2,5-F$_2$), $[Ru_2^{II,II}(2,3,5\text{-}F_3PhCO_2)_4(THF)_2]$ (2,3,5-F$_3$)

The compounds were synthesized on the basis of a method reported by Furukawa and Kitagawa.[11] The procedure for ***o*-Cl** is described as a representative example. $[Ru_2^{II,III}(CH_3CO_2)_4(THF)_2]BF_4$ (335 mg, 0.5 mmol) and *o*-chlorobenzoic acid (313 mg, 2.0 mmol) were refluxed in *N*,*N*-dimethylaniline (NDMA, 20 mL) for 12 h. After removing the solvent *in vacuo*, the brown residue was washed with *n*-hexane (10 mL × 3) and dissolved in a minimum amount of THF. The red solution was filtered, layered with *n*-hexane and allowed to stand for at least one week, affording ***o*-Cl** as brown crystals.

Yield: 79%. Elemental analysis (%) calculated for $C_{36}H_{32}O_{10}Cl_4Ru_2$: C 44.64, H 3.33. Found: C 44.85, H 3.31. IR (KBr): $\nu(CO_2)$ = 1550, 1398 cm^{-1}. For ***m*-Cl**, yield: 64%. Elemental analysis (%) calculated for $C_{36}H_{32}O_{10}Cl_4Ru_2$: C 44.64, H 3.33. Found: C 44.55, H 3.44. IR (KBr): $\nu(CO_2)$, 1550, 1390 cm^{-1}. For **2,3-Cl_2**, yield: 63%. Elemental analysis (%) calculated for $C_{36}H_{28}O_{10}Cl_8Ru_2$: C 39.08, H 2.55. Found: C 39.11, H 2.76. IR (KBr): $\nu(CO_2)$ = 1548, 1407 cm^{-1}. For **2,4-Cl_2**, yield: 65%. Elemental analysis (%) calculated for $C_{36}H_{28}O_{10}Cl_8Ru_2$: C 39.08, H 2.55. Found: C 39.29, H 2.67. IR (KBr): $\nu(CO_2)$ = 1544, 1385 cm^{-1}. For **2,5-Cl_2**, yield: 88%. Elemental analysis (%) calculated for $C_{36}H_{28}O_{10}Cl_8Ru_2$: C 39.08, H 2.55. Found: C 39.46, H 2.62. IR (KBr): $\nu(CO_2)$ = 1549, 1399 cm^{-1}. For **2,6-Cl_2**, yield: 8%. Elemental analysis (%) calculated for $C_{36}H_{28}O_{10}Cl_8Ru_2$: C 39.08, H 2.55. Found: C 39.46, H 2.62. IR (KBr): $\nu(CO_2)$ = 1579, 1389 cm^{-1}. For **3,4-Cl_2**, yield: 59%. Elemental analysis (%) calculated for $C_{36}H_{28}O_{10}Cl_8Ru_2$: C 39.08, H 2.55. Found: C 39.04, H 2.72. IR (KBr): $\nu(CO_2)$ = 1544, 1401 cm^{-1}. For **3,5-Cl_2·0.8Hexane**, yield: 45%. Elemental analysis (%) calculated for $C_{40.8}H_{39.2}O_{10}Cl_8Ru_2$: C 41.69, H 3.36. Found: C 41.77, H 3.46. IR (KBr): $\nu(CO_2)$ = 1563, 1397 cm^{-1}. For **2,3,4-Cl_3**, yield: 12%. Elemental analysis (%) calculated for $C_{36}H_{24}O_{10}Cl_{12}Ru_2$: C 34.75, H 1.94. Found C 34.93, H 2.10. IR (KBr): $\nu(CO_2)$ = 1575, 1395 cm^{-1}. For **2,3,5-Cl_3·0.8Hexane**, yield: 36%. Elemental analysis (%) calculated for $C_{40.8}H_{35.2}O_{10}Cl_8Ru_2$: C 37.32, H 2.70. Found: C 37.16, H 2.87. IR (KBr): $\nu(CO_2)$ = 1549, 1394 cm^{-1}. For **2,4,5-Cl_3**, yield: 36%. Elemental analysis (%) calculated for $C_{36}H_{24}O_{10}Cl_{12}Ru_2$: C 34.75, H 1.94. Found C 34.67, H 2.12. IR (KBr): $\nu(CO_2)$ = 1576, 1390 cm^{-1}. For **2,5-F_2·0.5THF**, yield: 67%. Elemental analysis (%) calculated for $C_{38}H_{32}F_8O_{10.5}Ru_2$: C 44.80, H 3.17. Found: C 44.79, H 3.34. IR (KBr): $\nu(CO_2)$ = 1560, 1383 cm^{-1}. For **2,3,5-F_3**, yield: 21%. Elemental analysis (%) calculated for $C_{36}H_{24}F_{12}O_{10}Ru_2$: C 41.31, H 2.31. Found: C 41.46, H 2.41. IR (KBr): $\nu(CO_2)$ = 1576, 1399 cm^{-1}.

Synthesis of $[Ru_2^{II,II}(3,4,5\text{-}Cl_3PhCO_2)_4(THF)_2]$ (3,4,5-Cl_3), $[Ru_2^{II,II}(2,3\text{-}F_2PhCO_2)_4(THF)_2]$ (2,3-F_2), $[Ru_2^{II,II}(2,4\text{-}F_2PhCO_2)_4(THF)_2]$ (2,4-F_2)

The compounds were synthesized step-by-step via a ligand substitution process involving $[Ru_2^{II,III}]^+$, followed by reduction to the corresponding $[Ru_2^{II,II}]$ products.[12] As a representative example, the procedure for **2,3-F_2** is described. $[Ru_2^{II,III}(CH_3CO_2)_4Cl]$ (200 mg, 0.42 mmol) and 2,3-difluorobenzoic acid (537 mg, 3.4 mmol) were refluxed in a 1:1 solution of MeOH and H_2O (20 mL) for 12 h under aerobic conditions to synthesize $[Ru_2^{II,III}(2,3\text{-}F_2PhCO_2)_4Cl]$. The obtained red precipitate was collected by filtration, washed with water and dried *in vacuo*. Without further purification, a THF solution (15 mL) of the crude product and Zn powder (52 mg, 0.80 mmol) was stirred for 24 h under a nitrogen atmosphere. During this time, most of the solid dissolved. The reddish-coloured solution was filtered, and the filtrate was layered with *n*-hexane and allowed to stand for at least one week, affording **2,3-F_2** as brown crystals. Yield: 88%. Elemental analysis (%) calculated for $C_{36}H_{28}O_{10}F_8Ru_2$: C 44.36, H 2.90. Found: C 43.96, H 3.01. IR (KBr): $\nu(CO_2)$ = 1560, 1394 cm^{-1}. For **2,4-F_2**, yield: 68%. Elemental analysis (%) calculated for $C_{36}H_{28}O_{10}F_8Ru_2$: C 44.36, H 2.90. Found: C 44.32, H 2.97. IR (KBr): $\nu(CO_2)$ = 1560, 1395 cm^{-1}. For **3,4,5-Cl_3**, yield: 24.6%. Elemental analysis (%) calculated for $C_{36}H_{24}O_{10}Cl_{12}Ru_2$: C 34.75, H 1.94. Found C 34.64, H 2.08. IR (KBr): $\nu(CO_2)$ = 1539, 1379 cm^{-1}.

Synthesis of $[Ru_2^{II,II}(p\text{-}ClPhCO_2)_4(THF)_2]$ (*p*-Cl)

This compound was synthesized by a modified version of that for **3,4,5-Cl_3**, **2,3-F_2** and **2,4-F_2** because the solid product $[Ru_2^{II,III}(p\text{-}ClPhCO_2)_4Cl]$ has low solubility in THF. $[Ru_2^{II,III}(CH_3CO_2)_4Cl]$ (570 mg, 1.2 mmol) and *p*-chlorobenzoic acid (1497 mg, 9.6 mmol) were refluxed in a 1:1 solution of MeOH and H_2O (120 mL) for 12 h under aerobic conditions to synthesize $[Ru_2^{II,III}(p\text{-}ClPhCO_2)_4Cl]$.

The obtained red precipitate was collected by filtration, washed with water and dried *in vacuo*. Without further purification, a solution of the crude product and Zn powder (288 mg, 4.4 mmol) in THF (100 mL) was refluxed for 24 h under a nitrogen atmosphere. The reddish-coloured solution immediately underwent hot filtration. Once the filtrate was cooled to room temperature, it was layered with *n*-hexane and allowed to stand for several days, affording ***p*-Cl·THF** as brown crystals. Yield: 78%. Elemental analysis (%) calculated for $C_{40}H_{40}O_{11}Cl_4Ru_2$: C 46.16, H 3.87. Found: C 46.50, H 3.86. IR (KBr): $\nu(CO_2)$ = 1547, 1403 cm^{-1}.

Synthesis of $[Ru_2^{II,II}(2,3,4,5\text{-}Cl_4PhCO_2)_4(THF)_2]$ (2,3,4,5-Cl_4)

This compound was synthesized by a modified version of that for ***p*-Cl**, where a pure MeOH solution was used for the solvent in the ligand substitution process. $[Ru_2^{II,III}(CH_3CO_2)_4Cl]$ (479 mg, 1.0 mmol) and 2,3,4,5-tetrachlorobenzoic acid (1039 mg, 4 mmol) were refluxed in MeOH (50 mL) for 48 h under aerobic conditions to synthesize $[Ru_2^{II,III}(2,3,4,5\text{-}Cl_4PhCO_2)_4Cl]$. The obtained red precipitate was collected by filtration, washed with water and dried *in vacuo*. Without further purification, a solution of the crude product and Zn powder (130 mg, 2.0 mmol) in THF (40 mL) was refluxed for 24 h under a nitrogen atmosphere. The reddish-coloured solution immediately underwent hot filtration. The filtrate was then layered with *n*-hexane and allowed to stand for one week, affording **2,3,4,5-Cl_4·THF** as brown crystals. Yield: 84%. Elemental analysis (%) calculated for $C_{40}H_{28}O_{11}Cl_{16}Ru_2$: C 33.11, H 1.94. Found: C 33.11, H 2.06. IR (KBr): $\nu(CO_2)$ = 1582, 1375 cm^{-1}.

General Physical Measurements

Infrared spectra were measured on KBr disks with a Jasco FT-IR 620 spectrometer. Magnetic susceptibility measurements were conducted with a Quantum Design SQUID magnetometer

(MPMS-XL) at temperature ranges of 1.8–300 K and applying a magnetic field of 0.1 T, for which polycrystalline samples embedded in liquid paraffin were used. Experimental data were corrected for diamagnetic contributions of the sample holder and liquid paraffin using evaluated Pascal constants.[13] Cyclic voltammograms (CVs) were recorded in THF with tetra-*n*-butylammonium hexafluorophosphate (*n*-$Bu_4N(PF_6)$, 0.1 M) as the supporting electrolyte under a nitrogen atmosphere using an ALS/[H] CH Instruments Electrochemical Analyzer Model 600A. CVs of the solvent with only the supporting electrolyte were measured first. The desired compounds were then added to this solution ([Compound] = 1×10^{-3} M), and the CVs were acquired using a glassy carbon electrode as the working electrode, a Pt counter electrode and a $Ag/AgNO_3$ reference electrode. Finally, CV potentials were adjusted with the ferrocene/ferrocenium couple as an internal standard (Fc/Fc^+ = 213 mV (ΔE = 91 mV) in THF vs. Ag/Ag^+).

Crystallography

Crystal data were collected on a Rigaku Saturn CCD area detector with a graphite or multi-layer mirror monochromated Mo-Kα radiation (λ = 0.71075 Å). The structures were solved by direct methods (SHELXL 97,[14] SIR2008,[15] SIR92,[16] SIR2002[17] and SIR2004[18]) or by the heavy-atom Patterson method (PATTY) [19] and expanded using Fourier techniques (DIRDIF99). [20] All non-hydrogen atoms were anisotropically refined. Hydrogen atoms were introduced as fixed contributors. Full-matrix least-squares refinements on F^2 were based on observed reflections and variable parameters and converged with unweighted and weighted agreement factors of $R1 = \Sigma||F_o|-|F_c||/\Sigma|F_o|$ ($I > 2.00\sigma(I)$) and $wR2 = [\Sigma w(F_o^2-F_c^2)^2/\Sigma w(F_o^2)^2]^{1/2}$ (all data). All calculations were performed using the CrystalStructure crystallographic software package.[21] Details of the crystal structure analyses are summarized in Table S1.

Computational Details

Theoretical *ab initio* calculations were performed using the density functional theory (DFT) formalism, as implemented in the Gaussian 09 software,[22] employing Beck's three-parameter hybrid functional with the correlation functional of Lee, Yang and Parr (B3LYP).[23] Unrestricted open-shell calculations were performed for the molecule containing [Ru_2] units. The effective core potential basis function LanL2TZ with polarization (LanL2TZ(f))[24] for Ru atoms and 6-31G basis sets with polarization and diffuse functions (6-31+G(d))[25] for C, H, F, Cl and O atoms were adopted. In the calculations, spin polarization with S_Z = 1 (triplet spin multiplicity) for [Ru_2] units was used. The atomic coordinates determined using X-ray crystallography were used in the calculations.

Results and Discussion

Syntheses and Characterization

Most of the compounds in the Cl-substituted [$Ru_2^{II,II}$] series were synthesized by a one-pot reaction using NDMA as both the solvent and the reducing agent.[11] However, several compounds were synthesized in higher yields through a carboxylate ligand substitution reaction from $[Ru^{II,III}(CH_3CO_2)_4]^+$ to the desired benzoic acid derivatives followed by reduction with Zn.[12] Note that except for **2,6-Cl_2**, we were not able to synthesize [$Ru_2^{II,II}(Cl_xPhCO_2)_4$] ($x \geq 2$) with Cl_x-substituted benzoate ligands where both *ortho*-positions (i.e. positions 2 and 6, see Chart 1) are occupied by Cl atoms, although the corresponding [$Ru_2^{II,II}(F_xPhCO_2)_4$] compounds (**2,6-$F_2$**, **2,3,6-$F_3$**, **2,4,6-$F_3$**, **2,3,5,6-$F_4$** and **$F_5$**) were successfully obtained.[7] Indeed, even **2,6-Cl_2** was obtained in a low yield (8%). This could be attributed to the difference in the steric effect of the *ortho*-positions between Cl- and F-substituted groups explained as follows: many compounds having substituents at

the *ortho*-positions result in a large dihedral angle between the phenyl ring of the benzoate group and the plane composed of the bridging carboxylate and Ru metals (θ, Table 1) due to steric hindrance between the *ortho*-substituents and the oxygen atoms of the bridging carboxyl group. Furthermore, although $\theta \approx 90°$ reduces the steric hindrance between the *ortho*-substituents and the oxygen atoms of the bridging carboxyl group, another type of steric hindrance is possible, which is caused by the *ortho*-substituents of neighbouring benzoate moieties on a $[Ru_2^{II,II}]$ complex. This should be much more pronounced in the Cl-series than in the F-series because of longer C–Cl bond lengths and the larger atomic radius of Cl compared to F: this is one of the main reasons for the lower reactivity of 2,6-Cl substituted carboxylate ligands in the Cl-substituted series.

<<Insert Table 1 here>>

Structures

All compounds were structurally characterized by single-crystal X-ray crystallography. Figure1 shows ORTEP drawings of the structures of ***m*-Cl**, **2,3-Cl_2**, **2,3,4-Cl_3** and **2,3,4,5-Cl_4** as representative examples (other complexes are shown in Fig. S1). The bond lengths around the Ru centres for the present compounds are summarized in Table 1, together with reported previously relevant compounds.[7] Except for **2,5-Cl_2**, **2,6-F_2**, **2,3,5-F_3** and **2,3,4,5-F_4**, the diruthenium units have an inversion centre at the midpoint of the Ru–Ru bond. ***p*-Cl**, **2,5-Cl_2**, **2,6-Cl_2**, **3,4-Cl_2** and **F_5** contain two structurally independent units in a unit cell, which are very similar to each other. Except for **3,4-Cl_2** and **2,3,4-Cl_3**, the Ru–Ru bond length of the complexes is in the range of 2.260–2.280 Å, similar to those of previously reported $[Ru_2^{II,II}]$ compounds;[5,7,26] whereas **3,4-Cl_2** has slightly longer Ru–Ru bond lengths of 2.291 and 2.336 Å, and **2,3,4-Cl_3** has a much shorter bond length of 2.189 Å.

The Ru–O_{eq} (O_{eq} = equatorial oxygen atoms) bond length varies in the range of 2.05–2.07 Å, except for **2,3,4-Cl_3**, which shows a slightly longer Ru–O_{eq} bond length of 2.106 Å. For the [Ru_2] units, the Ru–O_{eq} bond distance is a good indicator for evaluating the oxidation state (Table 1). Generally, Ru–O_{eq} bond lengths are found in the range of 2.06–2.08 Å for [$Ru_2^{II,II}$] and in the range of 2.02–2.04 Å for [$Ru_2^{II,III}$]$^+$.[5,7,26] Hence, all compounds should have the oxidation state of [$Ru_2^{II,II}$], including **2,3,4-Cl_3**, as proved by its magnetic properties (see below). Bond lengths of ca. 2.25–2.35 Å involving axial THF (Ru–O_{ax}) are also characteristic to the [$Ru_2^{II,II}$] valence state.

<<Insert Fig. 1 here>>

The dihedral angle (θ) is critical for the electronic effect that should mainly be given by benzoate substituents to Ru sites; the electronic conjugation between the phenyl ring and the carboxyl group becomes most effective when $\theta = 0$, while substituent groups at the *ortho*-positions mostly result in $\theta \neq 0$. As such, the Hammett law was not discussed for *ortho*-substituted aromatics. The values of θ for the Cl- and F-series are listed in Table 1. When the number of *ortho*-substituents defines the [Ru_2] units as non-*o*-Cl(F), mono-*o*-Cl(F) and di-*o*-Cl(F), the average θ value for each group is 9.1 ± 6.0°, 31.0 ± 16.2° and 57.9 ± 28.1° for non-*o*-Cl, mono-*o*-Cl and di-*o*-Cl, respectively, and 16.2 ± 6.9°, 18.3 ± 8.7° and 43.1 ± 16.0° for non-*o*-F, mono-*o*-F and di-*o*-F, respectively. Clearly, Cl-substitutions result in larger θ values than the corresponding F-substitutions. In addition, the larger standard deviation in the Cl-series demonstrates that both intra- and inter-molecular steric hindrances could be critical, most likely due to the unique characteristics found in the Cl-series, such as longer C–Cl bond lengths and the larger atomic radius of Cl.

Magnetic Properties

The oxidation state of the [Ru_2] unit and its electron configuration on the frontier orbitals made by Ru–Ru bonding can be easily determined by measuring the magnetic properties of the compounds. The temperature dependence of the dc susceptibility (χ) of all compounds was measured on polycrystalline samples in the temperature range of 1.8–300 K at 0.1 T (the χ and χT vs T plots are shown in Fig. S2). The χT values at 300 K were determined to be in the range of 0.90–1.04 cm^3 K mol^{-1}, which decreased smoothly upon cooling to be in the range of 1.04×10^{-2}–5.18×10^{-2} cm^3 K mol^{-1} at 1.8 K. On the other hand, the χ value at 300 K gradually increased upon decreasing the temperature to about 100 K and reached a plateau, followed by an increase at temperatures below approximately 10 K. These features of the χ and χT vs. T plots are consistent with those for isolated [$Ru_2^{II,II}$] complexes with an S = 1 ground state affected by strong zero-field splitting (ZFS; $D \approx$ 230–320 cm^{-1} for general [$Ru_2^{II,II}$] complexes),[7, 27, 28] even though the increase of χ at low temperatures is ascribed to paramagnetic impurities such as [$Ru_2^{II,III}$]$^+$ species with S = 3/2. Thus, the magnetic data were simulated using a Curie paramagnetic model with S = 1, taking into account ZFS, temperature-independent paramagnetism (TIP) and an impurity with S = 3/2 (ρ).[29] The intermolecular interaction (zJ) was considered for many cases of magnetically isolated or weakly interacting [$Ru_2^{II,II}$] complexes in the framework of the mean-field approximation[30] but was not required in the present case to obtain an adequate fit ($zJ \approx 0$ for all complexes). The best fit of parameters for the compounds are listed in Table S2, where the g value was fixed to 2.00. The estimated D value is typical for general [$Ru_2^{II,II}$] species.[7,27,28] The magnetic data indicate that all complexes have an electron configuration of $\sigma^2\pi_2^4\delta^2\delta^{*2}\pi^*_2{}^2\sigma^{*0}$ on Ru–Ru bond frontier orbital sets with degenerated levels of δ^* and two π^* orbitals.

Electrochemistry in Solution

CVs of the compounds were measured in N_2-saturated THF solutions with *n*-$Bu_4N(PF_6)$ as the supporting electrolyte and Ag/Ag^+ as the reference electrode, as shown in Fig. 2. For all compounds, a reversible one-electron redox wave assigned to $[Ru_2^{II,II}]/[Ru_2^{II,III}]^+$ was observed, with $I_c/I_a \approx 1$ and $\Delta E_p \approx 85–171$ mV for the Cl-series and $\Delta E_p \approx 47–183$ mV for the F-series, including previously reported compounds.[7] The redox potential ($E_{1/2}$) was observed over a wide range of potentials from 22 to 337 mV for the Cl-series and -39 to 360 mV for the F series, showing the substituent effect even between the Cl- and F-series. The electrochemical data are summarized in Table 2 along with the pK_a of the corresponding benzoic acids and the summation of the Hammett constants for *m*- and *p*-Cl(F) groups, as well as $\Sigma(x\sigma_m + y\sigma_p)$, where $\sigma_m = 0.373$ and $\sigma_p = 0.227$ for the Cl-series and $\sigma_m = 0.337$ and $\sigma_p = 0.062$ for the F-series. *x* and *y* represent the number of *m*- and *p*-substituents present, respectively.[31] One of the most pronounced effects on the substituents of benzoate moieties emerges from their pK_a values, and this relationship is known as the Hammett law. The pK_a values of substituted benzoate moieties is directly associated with the electronic effect that is propagated from the carboxylate group to the Ru centres in the compound. Thus, I_D for $[Ru_2^{II,II}]$ units and $E_{1/2}$ of $[Ru_2^{II,II}]/[Ru_2^{II,III}]^+$ states are functions of the substituent effect of benzoate bridging moieties in $[Ru_2^{II,II}]$; a stronger electron-withdrawing character of the substituents makes it difficult to release an electron from its $[Ru_2^{II,II}]$ unit to derive a higher I_D and $E_{1/2}$.

<<Insert Fig. 2 here>>

<<Insert Table 2 here>>

Figure 3 shows plots of $E_{1/2}$ values as a function of pK_a of the corresponding benzoic acids (i.e.

Cl_xPhCO_2H and F_xPhCO_2H), where Fig. 3a is the Cl-series and Fig. 3b is the F-series. The $E_{1/2}$ vs. pK_a relationship is very clear in each series, which should be compared as non-*o*-Cl(F), mono-*o*-Cl(F) and di-*o*-Cl(F) in order to exclude the effect of steric hindrance on *ortho*-substitutions (see the structural description), confirming a linear relationship for each group (except for di-*o*-Cl with only one plot of **2,6-Cl_2**). Note that the slopes of the linear relationships in the series are nearly identical. The effect on *ortho*-substitutions, which includes both structural and electronic effects, equally affect each group; in other words, the slope of the linear relationship in each group can only be decided by the electronic effect on *meta*- and *para*-substitutions, as described by the Hammett law (see below). The change in pK_a between neighbouring lines (ΔpK_{a1} between the lines of non-*o*-Cl(F) and mono-*o*-Cl(F), ΔpK_{a2} between the lines of mono-*o*-Cl(F) and di-*o*-Cl(F)) are almost identical, i.e. $\Delta pK_{a1} \approx \Delta pK_{a2}$, indicating that the electronic effects on *ortho*-substituents are more pronounced than the steric effects in solution, or the steric effects are proportional to the number of *ortho*-substituents in solution.

<<Insert Fig. 3 here>>

$E_{1/2}$ was plotted as a function of $\Sigma(x\sigma_m + y\sigma_p)$, as shown in Figs. 4a and 4b for the Cl- and F-series, respectively. A linear trend was observed in non-, mono- and di-*o*-substitutions on the Cl- and F-series similar to their pK_a dependence. If the steric effect was negligible in solution, a change in $\Sigma(x\sigma_m + y\sigma_p)$ between neighbouring lines should have resulted from the electronic effects on *ortho*-substitutions (σ_o). Thus, we evaluated the Hammett constant (σ_o) for *o*-Cl and *o*-F substitutions as 0.272 and 0.217, respectively. This was accomplished by minimizing the error for the least-squares linear fit in the plot of $E_{1/2}$ vs. $\Sigma(x\sigma_m + y\sigma_p + z\sigma_o)$, as shown in Figs. 4c and 4d for the Cl- and F-series, respectively (R^2 = 0.976 and 0.866, respectively), where z is 0, 1 and 2 for the non-, mono- and

di-*o*-positioned substitutions, respectively. The estimated σ_o value, which is an intermediate between the Hammett constants σ_m and σ_p, is well suited to predict the $E_{1/2}$ values in the framework of Hammett analysis.

<<Insert Fig. 4 here>>

Finally, the $E_{1/2}$ vs. $\Sigma(x\sigma_m + y\sigma_p + z\sigma_o)$ plots for the Cl- and F-series, which were independently evaluated (Fig. 4c and Fig. 4d, respectively), were gathered into a plot to make a common diagram for $[Ru_2^{II,II}]$ complexes (Fig. S3). A linear relationship is still found in this case. This implies that the Hammett constants, σ_o(Cl) = 0.272 and σ_o(F) = 0.217, are still effective for predicting the redox potential for the $[Ru_2^{II,II}]$ units where both Cl- and F-substituents are mixed; however, the slope of the least-squares fit (see Fig. S3) varied slightly from the respective lines for the independently evaluated Cl- and F-series (Fig. 4c and 4d). This diagram is also expected to be valid for other substituents at the *meta*- and *para*-positions if their Hammett constants are available; for example, $[Ru_2(m\text{-}MePhCO_2)_4(THF)_2]$ and $[Ru_2(p\text{-}MePhCO_2)_4(THF)_2]$ (–99 and –116 mV in THF vs. Ag/Ag^+, respectively) were also plotted in Fig. S3. The same quantitative procedure discussed above was valid for various $[Ru_2]$ units for which *ortho*-positions of benzoate ligands were substituted with other groups, which may allow a common Hammett analysis using all substitutions, even at *ortho*-positions.

DFT Calculations from Crystal Structures

To determine the energy levels of the molecular orbitals (MOs) of the present compounds, calculations on the basis of density functional theory (DFT) were performed at the UB3LYP level

with basis functions LANL2TZ(f) for Ru and 6-31+g(d) for other atoms. Note that this calculation was also performed for the previously reported F-series complexes for comparison, as the calculation in the previous work was performed with a different basis set.[7] For all compounds except **2,3,4-Cl$_3$**, the HOMO level that is most likely involved in the $[Ru_2^{II,II}]/[Ru_2^{II,III}]^+$ couple was assigned as the $\delta^*(\beta)$ frontier orbital, whereas that for **2,3,4-Cl$_3$** corresponds to the $\pi^*(\beta)$ frontier orbital. The HOMO energy level of the complexes is listed in Table 3.

<<Insert Table 3 here>>

Figure 5 shows plots of the HOMO energy levels vs. pK_a of the corresponding ligands. A linear trend similar to that found in the plot of $E_{1/2}$ vs. pK_a (Fig. 3) was also observed; three groups of non-, mono- and di-*o*-substituted complexes were classified following respective quasi-linear relationships dependent on *m*- and *p*-substituents, where the solid line represents the least-squares fit for each group. Thus, the Cl- and F-substituent effects quantitatively influence the MO energy levels estimated by DFT calculations on the basis of solid-state structures. The HOMO level should be directly associated with the I_D of the complexes as well as $E_{1/2}$ of complexes. Therefore, investigating the relationship between the HOMO level and $E_{1/2}$ of a complex is essential for understanding the importance of I_D in a target complex. In addition, as the MO levels were evaluated on the basis of their solid-state structures, this investigation provides valuable information on the deviation of the HOMO level caused by the steric effect, i.e. it clarifies the difference between non-*o*-substituted groups and *o*-substituted groups. Plots of the HOMO energy level vs. $E_{1/2}$ for the Cl- and F-series are depicted in Fig. 6, where the solid line is the least-squares fit on the basis of the non-*o*-substituted group of each series. As the line for the non-*o*-substituted group was defined as the standard line that yields the

minimum contribution to the steric effect, most of the compounds having substituents at the *ortho*-positions deviate from the standard line, many of which are in the upper region. Note that the compounds lying far from the standard line tend to have large θ values (Fig. S4). This indicates that the HOMO level obtained by the DFT calculations reflects the steric effect, which is < 0.3 eV for the Cl-series and < 0.55 eV for the F-series. Complexes with a small θ are located near the line, although a few exceptions are present (Fig. S4). Thus, the steric effect was identified in the HOMO level, estimated from a static state of structure, whereas it could be quantitatively treated in the redox potential as if the steric effect on *ortho*-substitutions were negligible. This is most likely due to the fact that the benzoate ligand of the [Ru_2] complexes can rotate freely in solution even in *ortho*-substituted ligands. In such a case, the effect on *ortho*-substitutions could be regarded as the electronic effect. Considering the fact that the HOMO levels of the *ortho*-substituted groups include steric effects, the standard line given in Fig. 6 indicates a lower limit of HOMO levels of the [Ru_2] series in the solid-state.

<<Insert Fig. 5 here>>

<<Insert Fig. 6 here>>

Finally, for the sake of comparison between the Cl- and F-series, pK_a, $E_{1/2}$ and the HOMO level of the series were plotted as the Cl-series vs. the F-series, as shown in Fig. 7, where the solid black line with a slope of 1 is given as the substitution effects of Cl and F, which were considered to be identical. Fig. 7a clearly indicates that the acidity of the corresponding benzoic acid is stronger in the Cl-series than the F-series. This trend can also be predicted from the Hammett constants (σ_m, σ_p, σ_o = 0.373, 0.227, 0.272 and 0.337, 0.062, 0.217 for the Cl- and F-series, respectively) and can be roughly seen

for $E_{1/2}$, as shown in Fig. 7b, where the electron donating ability of the F-series is somewhat higher than that of the Cl-series in solution. This tendency is similar to the plot of the HOMO level (Fig. 7c), where most of the points are located in the lower right region, coloured in blue; however, due to the contribution of the steric effects, this is not certain.

<<Insert Fig. 7 here>>

It should be noted on the substitution effect in the vibrational modes of carboxylate groups of benzoate ligands, which can be confirmed in infrared spectra in the range of 1370–1420 cm^{-1} and 1530–1600 cm^{-1} for the symmetry (ν_{sym}) and asymmetry (ν_{asym}) stretching vibrations, respectively (see experimental section for the solid state of compounds); Fig. S5 shows the variation of frequencies of respective vibrational modes as a function of pK_a. While the symmetric mode has no significant shift in the entire series of compounds, the asymmetric mode seems to have a small pK_a dependency, namely the substitution effect. However, because of the presence of large errors among the series in addition to including the steric effect that induces large θ angles in the *ortho*-substituted groups, we abandoned to evaluate the substitution effect using the vibrational modes.

Conclusion

To gain deeper insight into the variation of the electron donating ability of paddlewheel-type diruthenium(II, II) complexes tuned by bridging carboxylate ligands, we focused on two types of series with Cl- and F-substituted benzoate bridging ligands, $[Ru_2(Cl_xPhCO_2)_4]$ and $[Ru_2(F_xPhCO_2)_4]$; these complexes were isolated as crystals and structurally, magnetically and electrochemically characterized. Analyses of the electron donating ability based on relevant parameters, pK_a, $E_{1/2}$, the

Hammett constant and the HOMO level calculated by DFT, revealed that the Cl- or F-substituent effect is in agreement with the electronic effect for [Ru_2] following a linear relationship, which can be treated in the framework of the general Hammett law. Note that quantitative analysis should be performed for complexes in solution, because the solid-state form of the complexes involves steric effects caused by *ortho*-substitution and/or intermolecular interactions. The HOMO levels calculated on the basis of solid-state structures, especially for the *ortho*-substituted complexes, involve error such as E_{HOMO} < 0.3 eV and < 0.55 eV for the Cl- and F-series, respectively. As predicted from the Hammett constant, the [Ru_2] complexes in the Cl-series have slightly lower electron donating abilities than those of the F-series, which is characteristic in complexes with one or two substitutions on a benzoate bridge. Thus, the present families of [$Ru_2(Cl_xPhCO_2)_4$] and [$Ru_2(F_xPhCO_2)_4$] act as good electron-donor units of which the donating ability can be accurately tuned over a wide range of $E_{1/2}$ = −50 –+350 mV and E_{HOMO} =−4.2 −-5.2 eV.

Acknowledgements. We thank Dr. Satoshi Matsunaga (Faculty of Science, Kanagawa University) for his help with compound synthesis. This work was supported by a Grant-in-Aid for Scientific Research (Grant No. 21350032, 26810029) from the Ministry of Education, Culture, Sports, Science and Technology, Japan, ICC-IMR, LC-IMR and The Asahi Glass Foundation.

Supporting Information Available.

CIF files for X-ray crystallographic data and figures for structures for the compounds, magnetic data, plot of half-wave redox potential ($E_{1/2}$) vs. Hammett constants, plot of HOMO level vs. $E_{1/2}$ with dihedral angles. This material is available free of charge via the Internet at http://pubs.acs.org.

Table 1. Relevant bond lengths (Å) around Ru centres and dihedral θ angles (°) between the least-squares planes defined by the phenyl ring of the benzoate ligand and the carboxylate-bridging mode (i.e. atom set of Ru_2O_2C) in $[Ru_2^{II,II}(Cl_xPhCO_2)_4(THF)_2]$ and $[Ru_2^{II,II}(F_xPhCO_2)_4(THF)_2]$ (Set-1–Set-4: benzoate ligands structurally determined as asymmetric groups).

Compound	Ru−Ru / Å	Averaged Ru-O_{eq} / Å	Ru−O_{ax} / Å	θ / °					Reference
				Set-1	Set-2	Set-3	Set-4	Average	
***o*-Cl**	2.2666(3)	2.065	2.325(2)	40.40	29.99			35.2	5g
***m*-Cl**	2.2682(3)	2.066	2.3254(19)	16.44	3.92			10.2	This work
***p*-Cl** (unit 1)	2.2691(6)	2.064	2.320(4)	6.38	6.61			6.5	This work
(unit 2)	2.2659(5)	2.067	2.301(4)	4.53	8.64			6.6	This work
2,3-Cl_2	2.2645(4)	2.066	2.306(3)	20.43	15.10			17.8	This work
2,4-Cl_2	2.2673(8)	2.068	2.322(5)	21.31	1.22			11.3	This work
2,5-Cl_2 (unit 1)	2.2664(3)	2.066	2.283[a]	18.57	28.37	8.44	27.90	20.8	This work
(unit 2)	2.2724(3)	2.060	2.304[a]	29.36	40.79	34.35	40.94	36.4	This work
2,6-Cl_2 (unit 1)	2.2699(6)	2.071	2.311(3)	79.62	34.71			57.2	This work
(unit 2)	2.2723(6)	2.065	2.344(4)	84.70	32.49			58.6	This work
3,4-Cl_2 (unit 1)	2.2911(10)	2.059	2.323(9)	7.95	4.52			6.2	This work
(unit 2)	2.3355(14)	2.046	2.303(14)	6.30	8.27			7.3	This work
3,5-Cl_2	2.2707(13)	2.066	2.320(3)	4.45	9.35			6.9	This work
2,3,4-Cl_3	2.1893(5)	2.106	2.254(3)	55.31	74.20			64.8	This work
2,3,5-Cl_3	2.2604(13)	2.062	2.306(5)	27.06	37.51			32.3	This work
2,4,5-Cl_3	2.2744(16)	2.062	2.349(4)	39.79	15.66			27.7	This work
3,4,5-Cl_3	2.2749(12)	2.065	2.330(5)	25.90	14.01			20.0	This work
2,3,4,5-Cl_4	2.2738(11)	2.063	2.305(7)	26.46	49.28			37.9	This work
***o*-F**	2.2649(8)	2.068	2.312(2)	37.49	17.69			27.6	7
***m*-F**	2.2691(4)	2.065	2.331(2)	3.17	19.52			11.3	7
***p*-F**	2.2677(2)	2.061	2.3537(15)	19.48	15.78			17.6	7
2,3-F_2	2.2684(6)	2.066	2.312(3)	21.86	16.07			19.0	This work
2,4-F_2	2.2686(5)	2.064	2.324(3)	21.99	7.82			14.9	This work
2,5-F_2	2.2669(10)	2.065	2.340(3)	9.49	11.47			10.5	This work
2,6-F_2	2.2706(2)	2.065	2.332[a]	41.99	32.68	31.25	43.65	37.4	7
3,4-F_2	2.2744(4)	2.064	2.354(3)	19.80	14.04			16.9	7
3,5-F_2	2.2708(8)	2.073	2.310(5)	20.11	8.08			14.1	7
2,3,4-F_3	2.2712(2)	2.066	2.3334(11)	22.62	17.68			20.2	7
2,3,5-F_3	2.2646(11)	2.059	2.308[a]	20.90	7.00	17.01	7.11	13.0	This work
2,3,6-F_3	2.2719(2)	2.070	2.3022(17)	61.17	41.92			51.6	7
2,4,5-F_3	2.2703(3)	2.068	2.329(2)	11.44	15.12			13.3	7
2,4,6-F_3	2.2723(2)	2.071	2.2829(16)	51.84	76.47			64.2	7
3,4,5-F_3	2.2767(5)	2.067	2.307(2)	18.22	27.78			23.0	7
2,3,4,5-F_4	2.2774(4)	2.068	2.299[a]	29.77	21.56	35.45	18.03	26.2	7
2,3,5,6-F_4	2.2731(3)	2.065	2.298(2)	36.68	26.34			31.5	7
F_5 (unit 1)	2.2754(7)	2.070	2.318(2)	25.84	33.43			29.6	7
(unit 2)	2.2804(8)	2.068	2.308(3)	42.00	38.67			40.3	7

[a]averaged value

Table 2. Electrochemical data of novel $[Ru_2^{II,II}(Cl_xPhCO_2)_4(THF)_2]$ and $[Ru_2^{II,II}(F_xPhCO_2)_4(THF)_2]$ compounds measured in THF containing 0.1 M *n*-$Bu_4N(PF_6)$ under N_2 (mV vs. Ag/Ag^+)[a].

Compound	E_a / mV	E_c / mV	$E_{1/2}$ / mV	ΔE_p / mV	I_a / I_c	pK_a of benzoate	$\Sigma(x\sigma_m + y\sigma_p)$[b]	$\Sigma(x\sigma_m + y\sigma_p + z\sigma_o)$[c]	Reference
***o*-Cl**	96	−14	41	121	1.01	2.94	0	0.272	This work
***m*-Cl**	134	38	86	107	1.01	3.83	0.373	0.373	This work
***p*-Cl**	102	−58	22	171	1.00	3.98	0.227	0.227	This work
2,3-Cl_2	200	107	154	104	1.18	2.53	0.373	0.645	This work
2,4-Cl_2	166	57	112	120	1.04	2.29	0.227	0.499	This work
2,5-Cl_2	216	118	167	109	1.02	2.51	0.373	0.645	This work
2,6-Cl_2	199	60	130	150	0.95	1.82	0.000	0.544	This work
3,4-Cl_2	160	67	112	104	0.95	3.60	0.600	0.600	This work
3,5-Cl_2	262	179	221	94	1.01	3.46	0.746	0.746	This work
2,3,4-Cl_3	278	201	240	88	1.06	2.23	0.600	0.872	This work
2,3,5-Cl_3	329	240	296	100	1.02	2.09	0.746	1.018	This work
2,4,5-Cl_3	272	180	226	103	1.03	2.25	0.600	0.872	This work
3,4,5-Cl_3	314	195	266	129	1.00	3.23	0.973	0.973	This work
2,3,4,5-Cl_4	374	300	337	85	0.96	1.80	0.973	1.245	This work
***o*-F**	84	−14	35	98	1.00	3.27	0	0.217	7
***m*-F**	99	−15	42	114	0.99	3.86	0.337	0.337	7
***p*-F**	11	−89	−39	100	0.99	4.14	0.062	0.062	7
2,3-F_2	142	46	93	106	0.97	2.93	0.337	0.554	This work
2,4-F_2	98	−29	35	138	1.00	3.21	0.062	0.279	This work
2,5-F_2	158	39	99	130	0.95	2.93	0.337	0.554	This work
2,6-F_2	115	−14	51	129	1.02	2.34	0	0.434	7
3,4-F_2	235	52	144	183	0.96	3.80	0.399	0.399	7
3,5-F_2	230	125	178	105	1.08	3.59	0.674	0.674	7
2,3,4-F_3	278	139	209	139	1.06	2.87	0.399	0.616	7
2,3,5-F_3	273	177	225	108	1.18	2.59	0.674	0.891	This work
2,3,6-F_3	394	277	336	117	1.01	2.00	0.337	0.771	7
2,4,5-F_3	263	164	214	99	1.01	2.87	0.399	0.616	7
2,4,6-F_3	244	99	172	145	1.10	2.28	0.062	0.496	7
3,4,5-F_3	334	213	274	121	1.06	3.46	0.736	0.736	7
2,3,4,5-F_4	383	246	315	137	1.09	2.53	0.736	0.953	7
2,3,4,5-F_4	412	308	360	104	1.00	1.66	0.674	1.108	7
F_5	429	287	358	142	0.99	1.60	0.736	1.170	7

[a]The ferrocene/ferrocenium couple, Fc/Fc^+ = 213 mV, was observed under the same conditions described in the Experimental Section. [b]σ_m = 0.373, σ_p = 0.227 for Cl and σ_m = 0.337, σ_p = 0.062 for F, from Ref. 31. [c]σ_o = 272 and 217 for Cl and F, respectively, were experimentally estimated.

Table 3. Calculated energy values of the HOMO level of $[Ru_2^{II,II}(Cl_xPhCO_2)_4(THF)_2]$ and $[Ru_2^{II,II}(F_xPhCO_2)_4(THF)_2]$ using the density functional theory (DFT) at the UB3LYP level with basis functions LANL2TZ(f) for Ru and 6-31+g(d) for other atoms, on the basis of the atomic coordinates determined by X-ray crystallography.

Compound	HOMO energy (eV)	Compound	HOMO energy (eV)
***o*-Cl**	−4.1677	***o*-F**	−4.1840
***m*-Cl**	−4.5323	***m*-F**	−4.4219
***p*-Cl**	−4.5048	***p*-F**	−4.5114
2,3-Cl_2	−4.5517	**2,3-F_2**	−4.5223
2,4-Cl_2	−4.6657	**2,4-F_2**	−4.4874
2,5-Cl_2	−4.5906	**2,5-F_2**	−4.6401
2,6-Cl_2	−4.4512	**2,6-F_2**	−4.3242
3,4-Cl_2	−4.7759	**3,4-F_2**	−4.7677
3,5-Cl_2	−4.9391	**3,5-F_2**	−4.9566
2,3,4-Cl_3	−5.1590	**2,3,4-F_3**	−4.9432
2,3,5-Cl_3	−4.9212	**2,3,5-F_3**	−4.8785
2,4,5-Cl_3	−4.9255	**2,3,6-F_3**	−4.6502
3,4,5-Cl_3	−5.0692	**2,4,5-F_3**	−4.8893
2,3,4,5-Cl_4	−5.0235	**2,4,6-F_3**	−4.7424
		3,4,5-F_3	−5.0679
		2,3,4,5-F_4	−5.0578
		2,3,5,6-F_4	−4.8518
		F_5	−5.1144

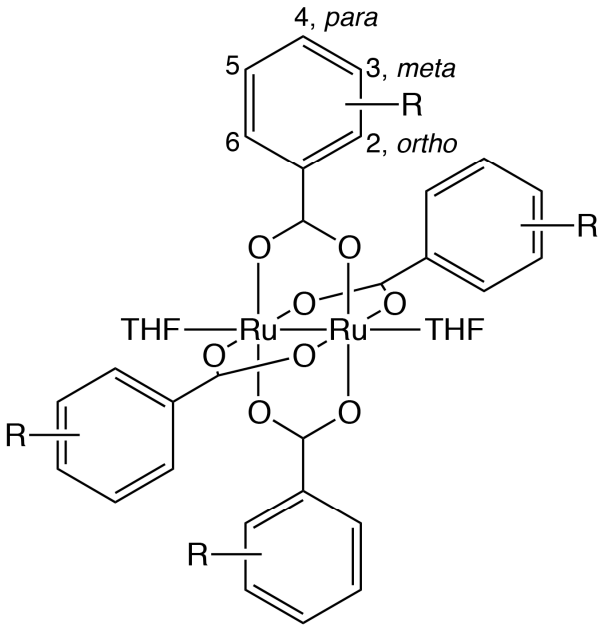

$[Ru_2^{II,II}(R_xPhCO_2)_4(THF)_2]$

$[Ru_2^{II,II}(Cl_xPhCO_2)_4(THF)_2]$

$[Ru_2^{II,II}(o\text{-}ClPhCO_2)_4(THF)_2]$ (***o*-Cl**)
$[Ru_2^{II,II}(m\text{-}ClPhCO_2)_4(THF)_2]$ (***m*-Cl**)
$[Ru_2^{II,II}(p\text{-}ClPhCO_2)_4(THF)_2]$ (***p*-Cl**)
$[Ru_2^{II,II}(2,3\text{-}Cl_2PhCO_2)_4(THF)_2]$ (**2,3-Cl$_2$**)
$[Ru_2^{II,II}(2,4\text{-}Cl_2PhCO_2)_4(THF)_2]$ (**2,4-Cl$_2$**)
$[Ru_2^{II,II}(2,5\text{-}Cl_2PhCO_2)_4(THF)_2]$ (**2,5-Cl$_2$**)
$[Ru_2^{II,II}(2,6\text{-}Cl_2PhCO_2)_4(THF)_2]$ (**2,6-Cl$_2$**)
$[Ru_2^{II,II}(3,4\text{-}Cl_2PhCO_2)_4(THF)_2]$ (**3,4-Cl$_2$**)
$[Ru_2^{II,II}(3,5\text{-}Cl_2PhCO_2)_4(THF)_2]$ (**3,5-Cl$_2$**)
$[Ru_2^{II,II}(2,3,4\text{-}Cl_3PhCO_2)_4(THF)_2]$ (**2,3,4-Cl$_3$**)
$[Ru_2^{II,II}(2,3,5\text{-}Cl_3PhCO_2)_4(THF)_2]$ (**2,3,5-Cl$_3$**)
$[Ru_2^{II,II}(2,4,5\text{-}Cl_3PhCO_2)_4(THF)_2]$ (**2,4,5-Cl$_3$**)
$[Ru_2^{II,II}(3,4,5\text{-}Cl_3PhCO_2)_4(THF)_2]$ (**3,4,5-Cl$_3$**)
$[Ru_2^{II,II}(2,3,4,5\text{-}Cl_4PhCO_2)_4(THF)_2]$ (**2,3,4,5-Cl$_4$**)

$[Ru_2^{II,II}(F_xPhCO_2)_4(THF)_2]$

$[Ru_2^{II,II}(o\text{-}FPhCO_2)_4(THF)_2]$ (***o*-F**)[a]
$[Ru_2^{II,II}(m\text{-}FPhCO_2)_4(THF)_2]$ (***m*-F**)[a]
$[Ru_2^{II,II}(p\text{-}FPhCO_2)_4(THF)_2]$ (***p*-F**)[a]
$[Ru_2^{II,II}(2,3\text{-}F_2PhCO_2)_4(THF)_2]$ (**2,3-F$_2$**)
$[Ru_2^{II,II}(2,4\text{-}F_2PhCO_2)_4(THF)_2]$ (**2,4-F$_2$**)
$[Ru_2^{II,II}(2,5\text{-}F_2PhCO_2)_4(THF)_2]$ (**2,5-F$_2$**)
$[Ru_2^{II,II}(2,6\text{-}F_2PhCO_2)_4(THF)_2]$ (**2,6-F$_2$**)[a]
$[Ru_2^{II,II}(3,4\text{-}F_2PhCO_2)_4(THF)_2]$ (**3,4-F$_2$**)[a]
$[Ru_2^{II,II}(3,5\text{-}F_2PhCO_2)_4(THF)_2]$ (**3,5-F$_2$**)[a]
$[Ru_2^{II,II}(2,3,4\text{-}F_3PhCO_2)_4(THF)_2]$ (**2,3,4-F$_3$**)[a]
$[Ru_2^{II,II}(2,3,5\text{-}F_3PhCO_2)_4(THF)_2]$ (**2,3,5-F$_3$**)
$[Ru_2^{II,II}(2,3,6\text{-}F_3PhCO_2)_4(THF)_2]$ (**2,3,6-F$_3$**)[a]
$[Ru_2^{II,II}(2,4,5\text{-}F_3PhCO_2)_4(THF)_2]$ (**2,4,5-F$_3$**)[a]
$[Ru_2^{II,II}(2,4,6\text{-}F_3PhCO_2)_4(THF)_2]$ (**2,4,6-F$_3$**)[a]
$[Ru_2^{II,II}(3,4,5\text{-}F_3PhCO_2)_4(THF)_2]$ (**3,4,5-F$_3$**)[a]
$[Ru_2^{II,II}(2,3,4,5\text{-}F_4PhCO_2)_4(THF)_2]$ (**2,3,4,5-F$_4$**)[a]
$[Ru_2^{II,II}(2,3,5,6\text{-}F_4PhCO_2)_4(THF)_2]$ (**2,3,5,6-F$_4$**)[a]
$[Ru_2^{II,II}(F_5PhCO_2)_4(THF)_2]$ (**F$_5$**)[a]

Chart 1. The series of $[Ru_2^{II,II}(Cl_xPhCO_2)_4(THF)_2]$ and $[Ru_2^{II,II}(F_xPhCO_2)_4(THF)_2]$ described here, where a) was referred from Ref. 7.

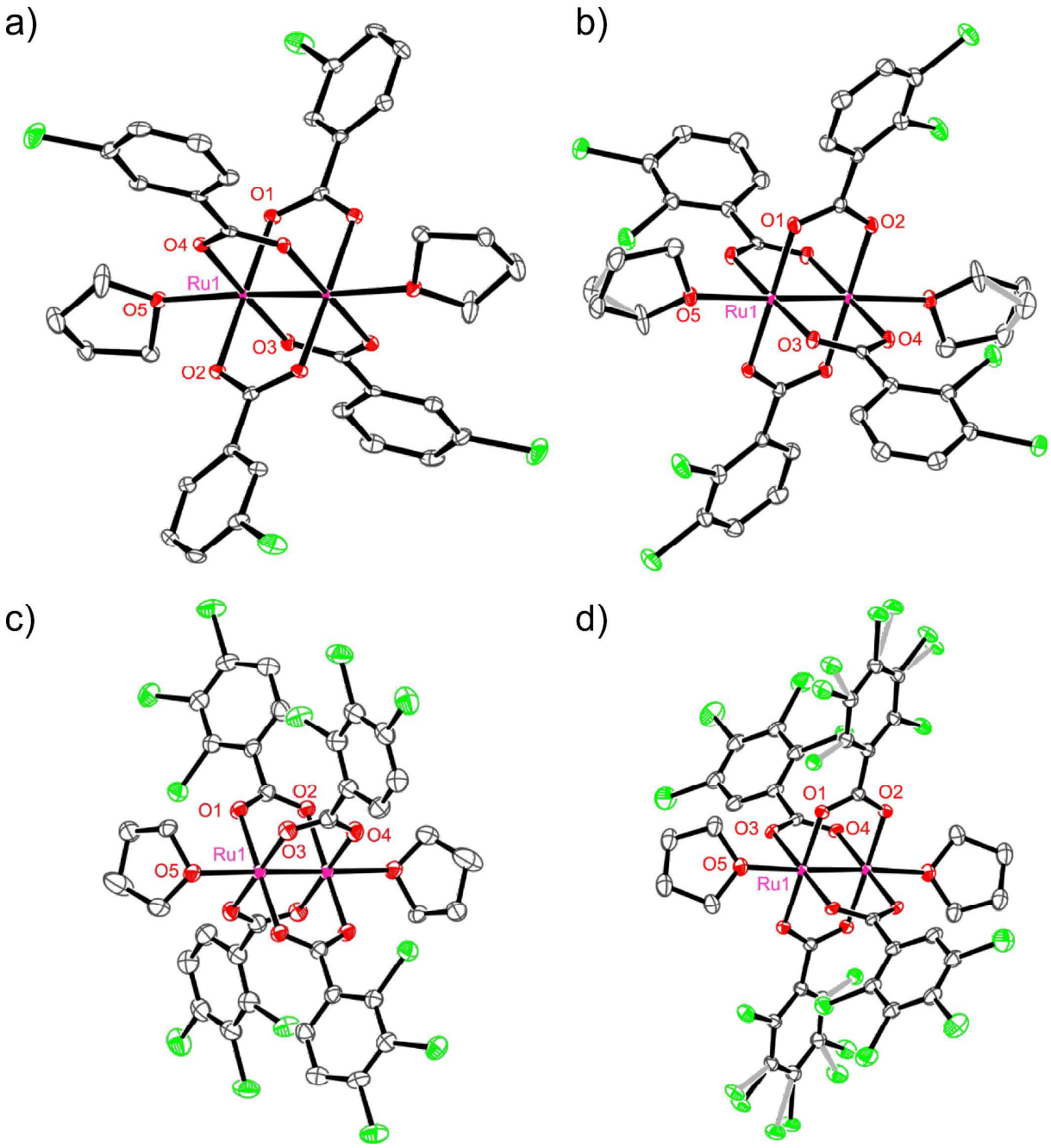

Fig. 1. ORTEP drawings of the structures of (a) ***m*-Cl**, (b) **2,3-Cl_2**, (c) **2,3,4-Cl_3** and (d) **2,3,4,5-Cl_4** (50% ellipsoid probability level), where red, grey, green and purple represent O, C, Cl and Ru, respectively, and the grey bonds represent disordered atomic positions. Hydrogen atoms were omitted for clarity.

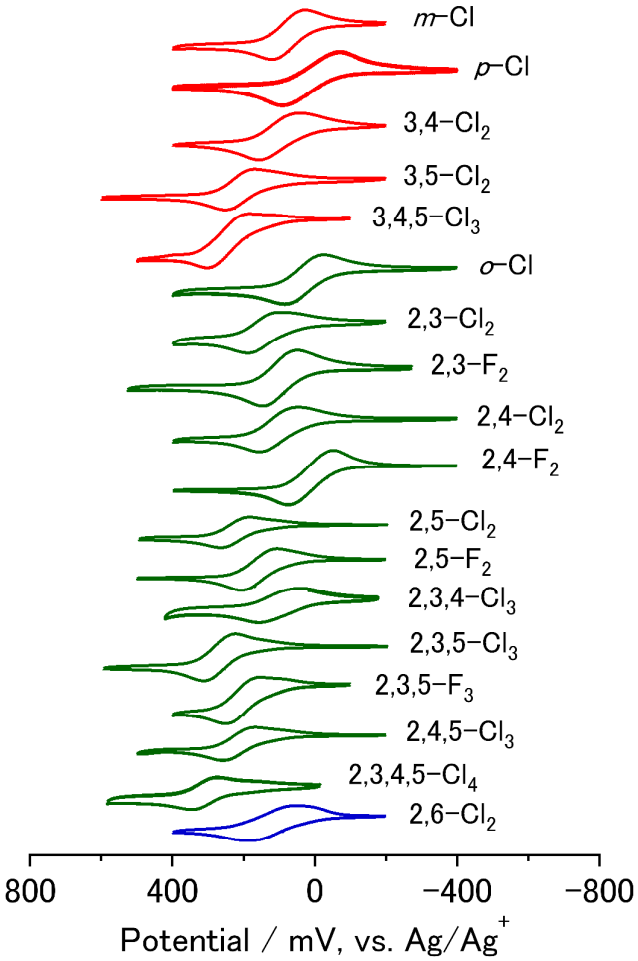

Fig. 2. CVs of newly synthesized $[Ru_2^{II,II}(Cl_xPhCO_2)_4(THF)_2]$ and $[Ru_2^{II,II}(F_xPhCO_2)_4(THF)_2]$ compounds in THF containing 0.1 M *n*-$Bu_4N(PF_6)$ under N_2, where non-, mono- and di-*ortho*-substituted groups were classified in colours of red, green and blue, respectively. The relevant values obtained from these CVs are summarized in Table 2.

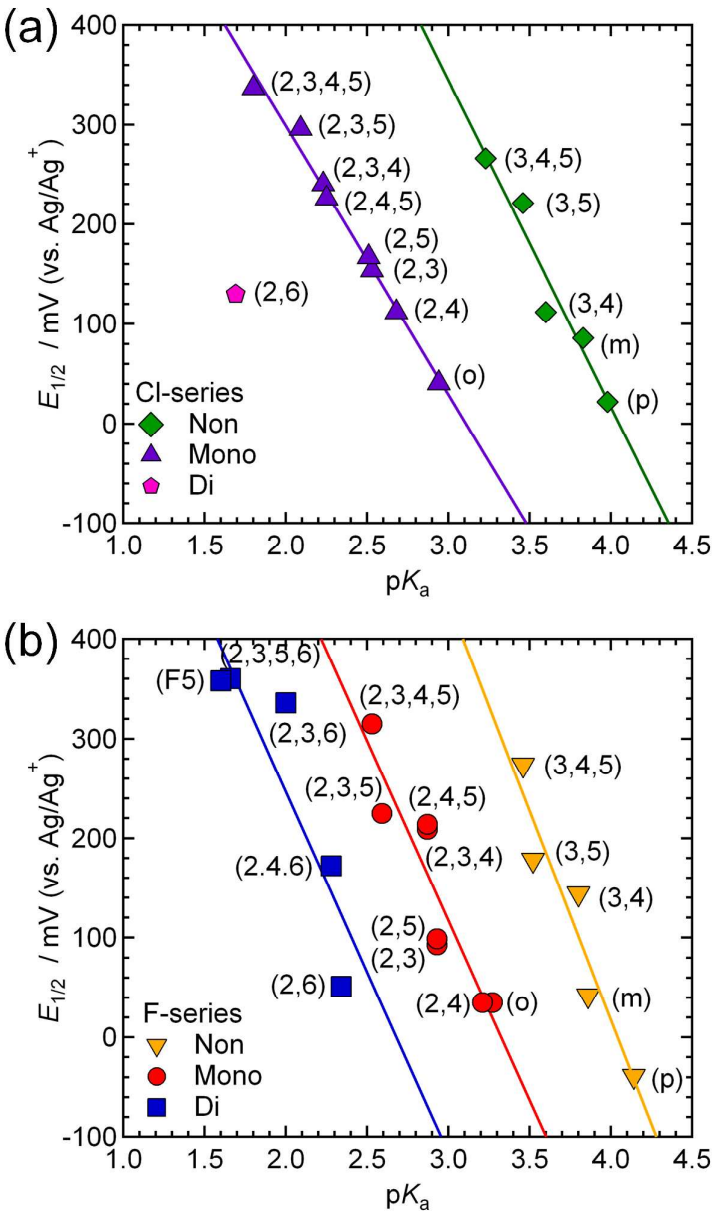

Fig. 3. Plots of half-wave redox potential ($E_{1/2}$) vs. pK_a for (a) the Cl-series and (b) the F-series, where the green (yellow), violet (red) and pink (blue) points represent non-Cl(F), mono-Cl(F) and di-*o*-Cl(F) substituted groups, respectively, and the solid lines represent the least-squares linear fit for the respective groups. $E_{1/2}$ and pK_a of all compounds are listed in Table 2.

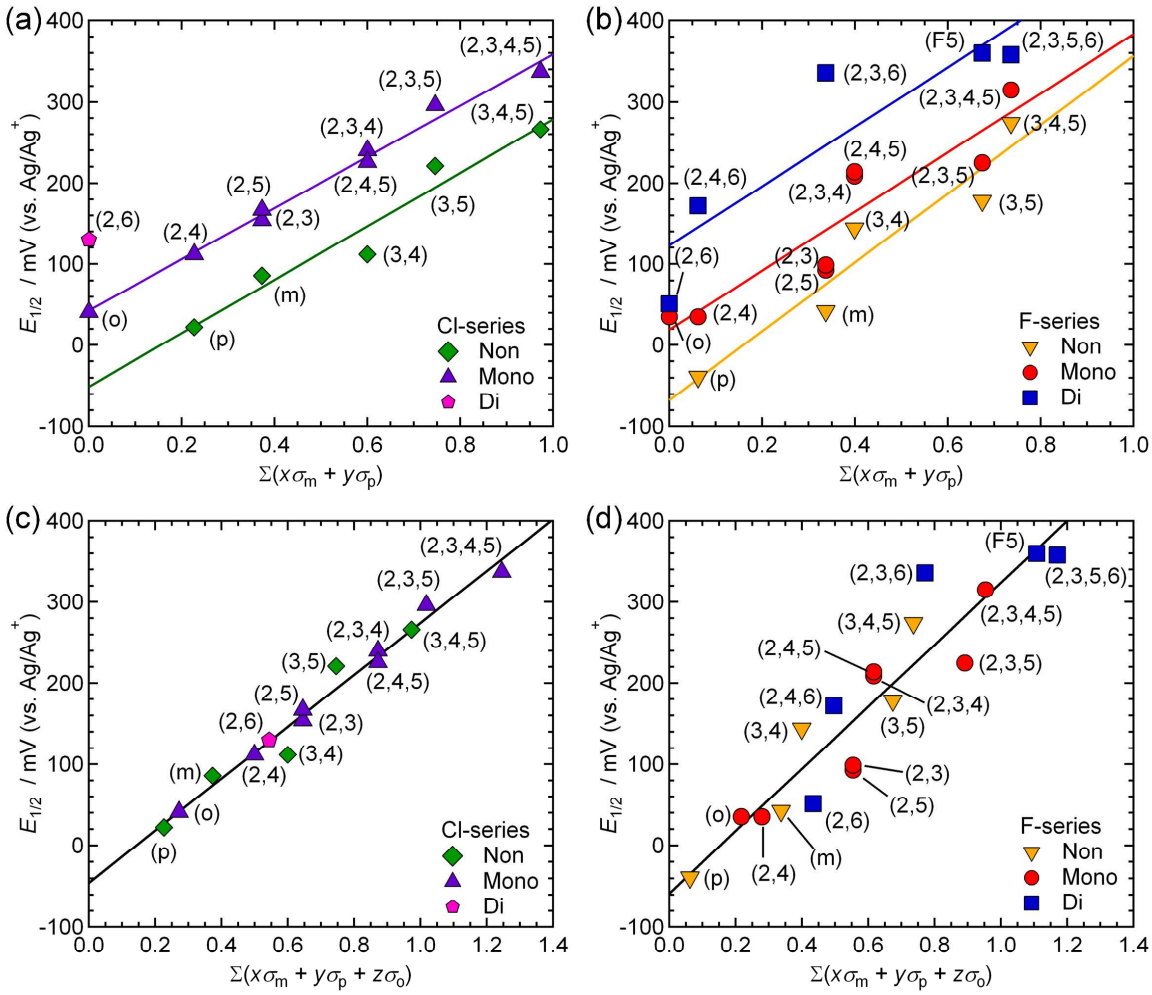

Fig. 4. Plots of (a and b) half-wave redox potential ($E_{1/2}$) vs. $\Sigma(x\sigma_m + y\sigma_p)$ and (c and d) $\Sigma(x\sigma_m + y\sigma_p + z\sigma_o)$ for (a, c) the Cl-series and (b, d) the F-series, respectively, where the green (yellow), violet (red) and pink (blue) points represent non-Cl(F), mono-Cl(F) and di-*o*-Cl(F) substituted groups, respectively, and the solid lines represent the least-squares fit for the respective plots. $E_{1/2}$ and the values of $\Sigma(x\sigma_m + y\sigma_p)$ and $\Sigma(x\sigma_m + y\sigma_p + z\sigma_o)$ of all compounds are listed in Table 2.

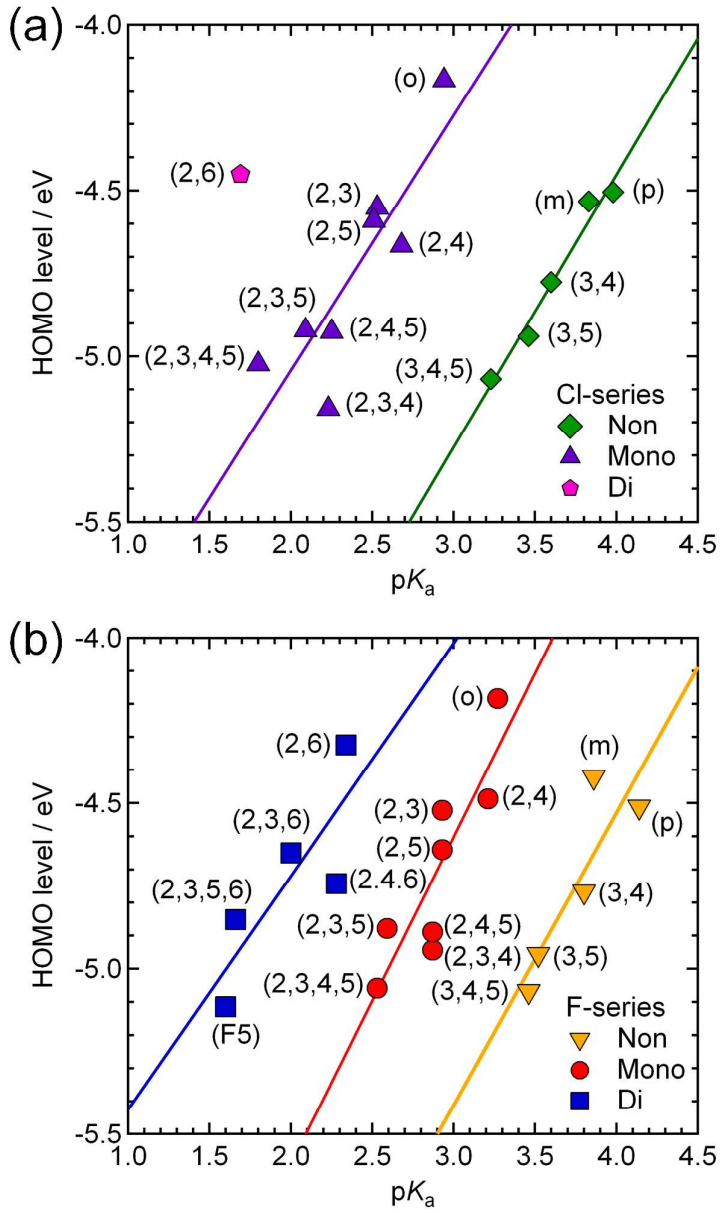

Fig. 5. Plots of HOMO level vs. pK_a for (a) the Cl-series and (b) the F-series, where the green (yellow), violet (red) and pink (blue) points represent non-Cl(F), mono-Cl(F) and di-*o*-Cl(F) substituted groups, respectively, and the solid lines represent the least-squares fit for the respective plots. The pK_a values and HOMO energy levels of all compounds are listed in Tables 2 and 3, respectively.

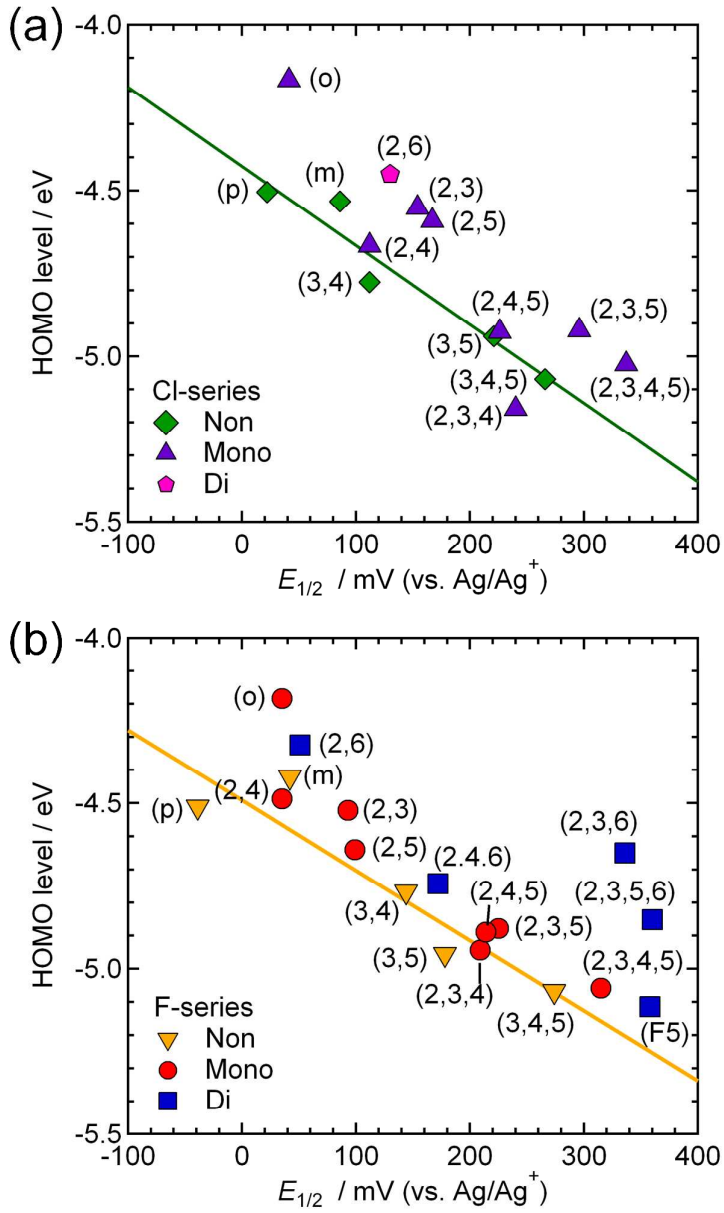

Fig. 6. Plots of HOMO level vs. $E_{1/2}$ for (a) the Cl-series and (b) the F-series, where the green (yellow), violet (red) and pink (blue) points represent non-Cl(F), mono-Cl(F) and di-*o*-Cl(F) substituted groups, respectively, and the solid lines represent the least-squares linear fit for the non-*o*-substituted groups in the respective series.

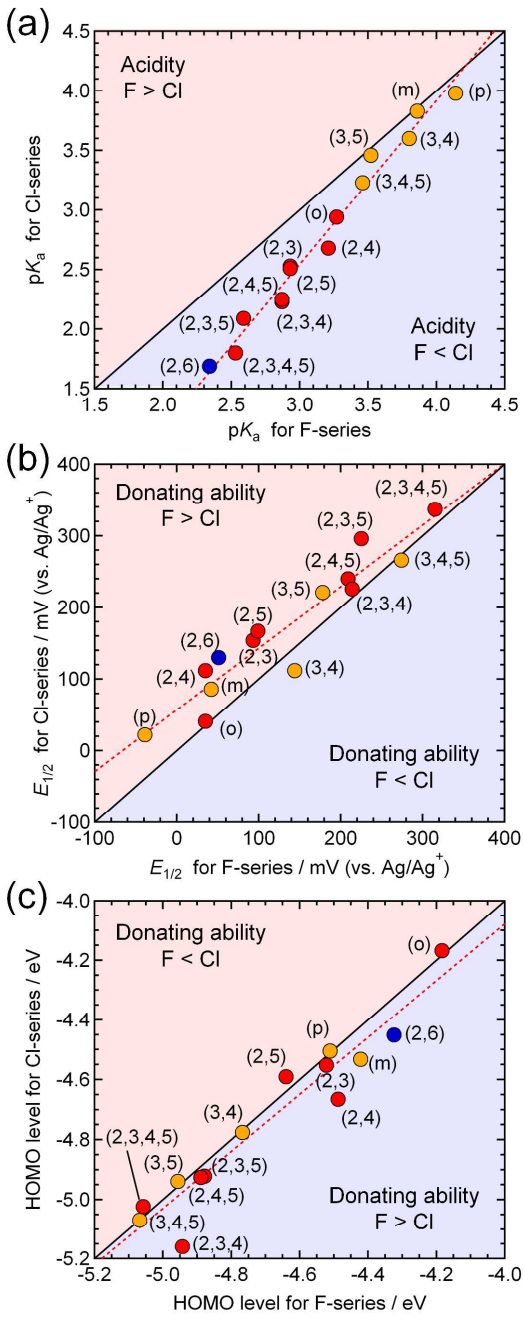

Fig. 7. Correlation diagrams between the Cl-series and the F-series with respect to (a) pK_a, (b) $E_{1/2}$ and (c) HOMO level, where the yellow, red and blue points represent the non-, mono- and di-*o* substituted groups, respectively. The black diagonal line with a slope of 1 indicates the neutral line that defines the identification of the Cl- and F-substitutions in the subject. The dotted lines represent the least-squares linear fit for the data.

Figure for contents

The effect of chlorine and fluorine substitutions on tuning the ionization potential of benzoate-bridged paddlewheel diruthenium(II, II) complexes

Wataru Kosaka, Masahisa Itoh and Hitoshi Miyasaka

A series of paddlewheel diruthenium(II, II) complexes with various chlorine- and fluorine-substituted benzoate ligands was summarized in viewpoints of their electrochemistry and HOMO level.

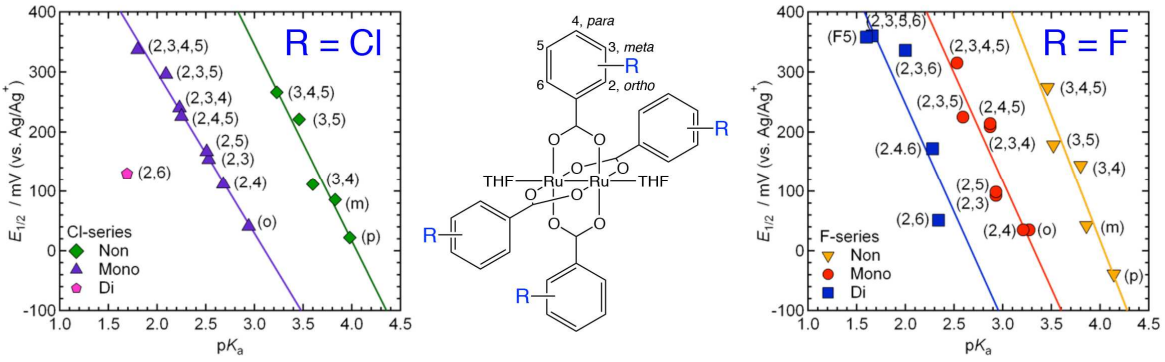

References

1 (a) J. S. Miller and A. J. Epstein, *Angew. Chem. Int. Ed. Engl.*, 1994, **33**, 385; (b) J. S. Miller, *Chem. Soc. Rev.*, 2011, **40**, 3266–3296.

2 (a) G. Saito and Y. Yoshida, *Bull. Chem. Soc. Jpn.*, 2007, **80**, 1; (b) N. Toyota, M. Lang and J. Müller, *Low-Dimensional Molecular Metals*, Springer, Heidelberg, 2007.

3 (a) F. Kagawa, S. Horiuchi, M. Tokunaga, J. Fujioka and Y. Tokura, *Nat. Phys.*, 2010, **6**, 169; (b) S. Horiuchi, R. Kumai, Y. Okimoto and Y. Tokura, *Chem. Phys.*, 2006, **325**, 78.

4 E. Collet, M.-H. Lemée-Cailleau, M. Buron-Le Cointe, H. Cailleau, M. Wulff, T. Luty, S.-Y. Koshihara, M. Meyer, L. Toupet, P. Rabiller and S. Techert, *Science*, 2003, **25**, 612.

5 (a) H. Miyasaka, C. S. Campos-Fernández, R. Clérac, K. R. Dunbar, *Angew. Chem. Int. Ed.*, 2000, **39**, 3831; (b) H. Miyasaka, T. Izawa, N. Takahashi, M. Yamashita and K. R. Dunbar, *J. Am. Chem. Soc.*, 2006, **128**, 11358; (c) N. Motokawa, T. Oyama, S. Matsunaga, H. Miyasaka, K. Sugimoto, M. Yamashita, N. Lopez and K. R. Dunbar, *Dalton Trans.*, 2008, 4099; (d) N. Motokawa, H. Miyasaka, M. Yamashita and K. R. Dunbar, *Angew. Chem. Int. Ed.*, 2008, **47**, 7760. (e) N. Motokawa, T. Oyama, S. Matsunaga, H. Miyasaka, M. Yamashita and K. R. Dunbar, *CrystEngComm*, 2009, **11**, 2121; (f) H. Miyasaka, N. Motokawa, S. Matsunaga, M. Yamashita, K. Sugimoto, T. Mori, N. Toyota and K. R. Dunbar, *J. Am. Chem. Soc.*, 2010, **132**, 1532; (g) N. Motokawa, S. Matsunaga, S. Takaishi, H. Miyasaka, M. Yamashita and K. R. Dunbar, *J. Am. Chem. Soc.*, 2010, **132**, 11943; (h) H. Miyasaka, T. Morita and M. Yamashita, *Chem. Commun.*, 2011, **47**, 271; (i) H. Miyasaka, N. Motokawa, T. Chiyo, M. Takemura, M. Yamashita, H. Sagayama and T. Arima, *J. Am. Chem. Soc.*, 2011, **133**, 5338; (j) K. Nakabayashi, M. Nishio, K. Kubo, W. Kosaka and H. Miyasaka, *Dalton Trans.*, 2012, **41**, 6072; (k) M. Nishio, N. Motokawa, M. Takemura and H. Miyasaka, *Dalton Trans.*, 2013, **42**, 15898; (l) H. Fukunaga, W. Kosaka and H. Miyasaka, *Chem. Lett.*, 2014, **43**, 541; (m) K. Nakabayashi and H. Miyasaka, *Chem. Eur. J.*, 2014, **20**, 5121; (n) M. Nishio, N. Hoshino, W. Kosaka, T. Akutagawa and H. Miyasaka, *J. Am. Chem. Soc.*, 2013, **135**, 17715; (o) M. Nishio, and H. Miyasaka, *Inorg. Chem.*, 2014, **53**, 4716; (p) H. Fukunaga and H. Miyasaka, *Angew. Chem. Int. Ed.*, 2014, **54**, 569.

6 H. Miyasaka, *Acc. Chem. Res.*, 2013, **46**, 248.

7 H. Miyasaka, N. Motokawa, R. Atsuumi, H. Kamo, Y. Asai and M. Yamashita, *Dalton Trans.*, 2011, **40**, 673.

8 F. A. Urbanos, M. C. Barral and R. Jiménez-Aparicio, *Polyhedron*, 1988, **7**, 2597.

9 R. W. Mitchell, A. Spencer and G. J. Wilkinson, *Chem. Soc., Dalton Trans.*, 1973, 846.

10 (a) T. M. A. Shaikh and A. Sudalai, *Eur. J. Org. Chem.*, 2008, 4877; (b) E. Dalcanale and F. Montanari, *J. Org. Chem.*, 1986, **51**, 567; (c) A. E. Jensen, W. dohle, I. Sapountzis, D. M. Lindsay, V. A. Vu and P. Knochel, *Synthesis*, 2002, 565.

11 S. Furukawa and S. Kitagawa, *Inorg. Chem.*, 2004, **43**, 6464.

12 F. A. Cotton, Y. Kim and A. Yokochi, *Inorg. Chim. Acta*, 1995, **236**, 55.

13 E. A. Boudreaux and L. N. Mulay, *Theory and Applications of Molecular Paramagnetism*, John Wiley and Sons, New York, 1976, 491.

14 G. M. Sheldrick, University of Gotingen, Germany, 1997.

15 M. C. Burla, R. Caliandro, M. Camalli, G. Carrozzini, L. De Caro, C. Giacovazzo, G. Polidori, D. Siliqi and R. Spagna, *J. Appl. Cryst.*, 2007, **40**, 609.

16 A. Altomare, G. Cascarano, C. Giacovazzo, A. Guagliardi, M. C. Burla, G. Polidori and M. Camalli, *J. Appl. Cryst.*, 1994, **27**, 435.

17 M. C. Burla, M. Camalli, B. Carrozzini, G. L. Cascarano, C. Giacovazzo, G. Polidori and R. Spagna, *J. Appl. Cryst.*, 2003, **36**, 1103.

18 M. C. Burla, M. Camalli, B. Carrozzini, G. L. Cascarano, C. Giacovazzo, G. Policori and R. Spagna, *J. Appl. Cryst.*, 2005, **38**, 381.

19 P. T. Beurskens, G. Admiraal, H. Behm, G. Beurskens, J. M. M. Smits and C. Z. Smykalla, *Kristallogr. Suppl.*, 1991, **4**, 99.

20 P. T. Beurskens, G. Admiraal, G. Beurskens, W. P. Bosman, R. de Gelder, R. Israel, J. M. M. Smits, (1999). The DIRDIF-99 program system, Technical Report of the Crystallography Laboratory, University of Nijmengen, The Netherlands.

21 CrystalStructure 4.0: Crystal Structure Analysis Package, Rigaku Corporation (2000 - 2010). Tokyo 196-8966, Japan.

22 M. J. Frisch, G. W. Trucks, H. B. Schlegel, G. E. Scuseria, M. A. Robb, J. R. Cheeseman, G. Scalmani, V. Barone, B. Mennucci, G. A. Petersson, H. Nakatsuji, M. Caricato, X. Li, H. P. Hratchian, A. F. Izmaylov, J. Bloino, G. Zheng, J. L. Sonnenberg, M. Hada, M. Ehara, K. Toyota, R. Fukuda, J. Hasegawa, M. Ishida, T. Nakajima, Y. Honda, O. Kitao, H. Nakai, T. Vreven, J. A. Montgomery, Jr., J. E. Peralta, F. Ogliaro, M. Bearpark, J. J. Heyd, E. Brothers, K. N. Kudin, V. N. Staroverov, R. Kobayashi, J. Normand, K. Raghavachari, A. Rendell, J. C. Burant, S. S. Iyengar, J. Tomasi, M. Cossi, N. Rega, J. M. Millam, M. Klene, J. E. Knox, J. B. Cross, V. Bakken, C. Adamo, J. Jaramillo, R. Gomperts, R. E. Stratmann, O. Yazyev, A. J. Austin, R. Cammi, C. Pomelli, J. W. Ochterski, R. L. Martin, K. Morokuma, V. G. Zakrzewski, G. A. Voth, P. Salvador, J. J. Dannenberg, S. Dapprich, A. D. Daniels, Ö. Farkas, J. B. Foresman, J. V. Ortiz, J. Cioslowski and D. J. Fox, *Gaussian 09, Revision B.01*, Gaussian, Inc., Wallingford CT, 2009.

23 A. D. Becke, *J. Chem. Phys.*, 1993, **98**, 5648.

24 (a) P. J. Hay and W. R. Wadt, *J. Chem. Phys.*, 1985, **82**, 299; (b) L. E. Roy, P. J. Hay, R. L. Martin, *J. Chem. Theory Comput.*, 2008, **4**, 1029; (c) A. W. Ehlers, M. Böhme, S. Dapprich, A. Gobbi, A. Höllwarth, V. Jonas, K. F. Köhler, R. Stegmann, A. Veldkamp and G. Frenking, *Chem. Phys. Lett.*, 1993, **208**, 111.

25 (a) P. C. Hariharan and J. A. Pople, *Theoret. Chimica Acta*, 1973, **28**, 213; (b) M. M. Francl, W. J. Petro, W. J. Hehre, J. S. Binkley, M. S. Gordon, D. J. DeFrees and J. A. Pople, *J. Chem. Phys.*, 1982, **77**, 3654; (c) T. Clark, J. Chandrasekhar and P. V. R. Schleyer, *J. Comp. Chem.*, 1983, **4**, 294; (d) R. Krishnam, J. S. Binkley, R. Seeger and J. A. Pople, *J. Chem. Phys.*, 1980, **72**, 650; (e) P. M. W. Gill, B. G. Johnson, J. A. Pople and M. J. Frisch, *Chem. Phys. Lett.*, 1992, **197**, 499.

26 F. A. Cotton and R. A. Walton, *Multiple Bonds between Metal Atoms*, second ed., Oxford University Press, Oxford, 1993.

27 (a) P. Maldivi, A.-M. Giroud-Godquin, J.-C. Marchon, D. Guillon and A. Skoulios, *Chem. Phys. Lett.*, 1989, **157**, 552; (b) F. A. Cotton, V. M. Miskowski and B. Zhong, *J. Am. Chem. Soc.*, 1989, **111**, 6177; (c) L. Bonnet, F. D. Cukiernik, P. Maldivi, A.-M. Giroud-Godquin and J.-C. Marchon, *Chem. Mater.*, 1994, **6**, 31; (d) E. V. Dikarev, A. S. Filatov, E. Clérac and M. A. Petrukhina, *Inorg. Chem.*, 2006, **45**, 744.

28 H. Miyasaka, R. Clérac, C. S. Campos-Fernández, K. R. Dunbar, *J. Chem. Soc., Dalton Trans.*, 2001, 858–861.

29 A. Cogne, E. Belorizky, J. Laugier and P. Rey, *Inorg. Chem.*, 1994, **33**, 3364.

30 C. J. O'Connor, *Prog. Inorg. Chem.*, 1982, **29**, 203.

31 L. P. Hammett, *J. Am. Chem. Soc.*, 1937, **59**, 96.